Characterization of Poly(lactic acid) Multifilament Yarns. I. The Structure and Thermal Behavior

M. Radjabian,[1] M. H. Kish,[1] N. Mohammadi[2]

[1]*Department of Textile Engineering, Amirkabir University of Technology (Tehran Polytechnic), Tehran 15875-4413, Iran*
[2]*Department of Polymer Engineering, Amirkabir University of Technology (Tehran Polytechnic), Tehran 15875-4413, Iran*

Received 30 September 2009; accepted 20 December 2009
DOI 10.1002/app.32046
Published online 29 March 2010 in Wiley InterScience (www.interscience.wiley.com).

ABSTRACT: The structure and thermal behavior of poly(lactic acid) (PLA) multifilament yarns were studied by complementary techniques of differential scanning calorimetry (DSC), Fourier transform infrared (FTIR) spectroscopy, and wide angle X-ray diffraction (WAXD). As for PLA filaments, notable differences in the WAXD patterns, DSC curves, and FTIR spectra were observed. The combination of the WAXD and FTIR results showed that PLA samples with different crystallinity contain α-form crystal structure. The FTIR spectra of the filaments were analyzed to study their crystallinity and crystal structure. The total crystallinity of the PLA filaments was obtained from the percent area loss of the skeletal amorphous band at 955 cm^{-1}. Crystalline fraction from FTIR and DSC were comparable with each other. The C=O stretching region, which is sensitive to crystallization and dipole–dipole interactions, was evaluated to provide information about chain conformers and crystallinity of the samples. Depending on the processing conditions, double melting peaks were observed in the DSC curves of the samples. This exhibited the structural reorganization of the crystal phase during heating affected by heating and cooling rate. In the DSC curves of the nearly amorphous multifilament yarn, the exothermic peak observed right above the glass transition temperature (T_g) indicated two relaxed and deformed amorphous regions. However, the multifilament yarn with higher crystallinity showed just endothermic melting peak after its glass transition. © 2010 Wiley Periodicals, Inc. J Appl Polym Sci 117: 1516–1525, 2010

Key words: poly(lactic acid); structure; thermal behavior; differential scanning calorimetry; FTIR

INTRODUCTION

Poly(L-lactic acid) (PLLA) (—[CH(CH3)COO]*n*—) is a well-known biodegradable and biocompatible semicrystalline aliphatic polyester. It has attracted enormous attention in recent years due to its ease of production from renewable resources (mainly starch and sugar) and degradation to nontoxic materials. PLLA is produced via two conventional ways: Polycondensation of lactic acid and ring-opening polymerization of lactide, a chiral monomer that is produced by bacterial fermentation.[1,2] The polymer is relatively hard, with the glass transition and melting temperatures of 60–70°C and 150–170°C, respectively.[2] High mechanical strength, high modulus, and proper degradation time of PLLA make it appropriate thermoplastic polymer for either medical or textile fibers with industrial applications. Until the last decade, the applications of PLLA were mainly limited to biomedical such as tissue engineering, surgical suture, bone fixation devices, and controlled drug delivery systems, due to its high cost, low availability, and limited molecular weight. However, in the last few years, the discovery of new polymerization routes, allowed for the advancement of economical production of high molecular weight PLLA, which caused new potential applications as a commodity plastic in packaging, disposable, and other consumer materials.[2]

PLLA crystallizes at least in three forms of α, β, and γ depending on the crystallization and processing conditions.[3–6] In the late 1960s, De Santis and Kovacs[3] published the α form and proposed a pseudo-orthorhombic structure with two left-handed 10_3 helical conformation chains in antiparallel orientation passing through the unit cell. The α modification grows from the melt or solution spinning process at low temperatures or low draw ratio under low drawing temperatures. Eling et al.[4] reported the β polymorph as the second crystal form, which is characterized by a frustrated structure. The β crystal form is produced by stretching the α form or solution spinning at high temperatures or high draw ratio under high drawing temperatures.[4,5] In 1990, an orthorhombic unit cell for the β form containing six

Correspondence to: M. H. Kish (mhkish@aut.ac.ir).

left-handed 3_1 helical conformation chains passing through the unit cell was proposed.[5] Hoogsteen et al.[5] assigned the α structure to the folded-chain crystals and the β form to the fibrillar crystals. They explained that the helical conformations of the chains in the α and β structures have approximately the same energy, and the packing type allows for the existence of two different crystal modifications. In 2000, Cartier et al.[6] reported the third crystal structure for PLLA, namely γ form, obtained by epitaxial crystallization of PLLA on hexamethylbenzene containing two unparallel helices in an orthorhombic unit cell. Like other synthetic fibers, the crystal structure imposes restrictions on the movements and entanglements in the disordered region of the fibers, which changes the physical and the mechanical properties.

Physical, mechanical, and thermal properties of PLLA as a semicrystalline polymer, greatly depend on its crystal structure and morphology. In addition, the complex melting behavior of PLLA is considerably influenced by crystallization conditions.[7] Recently, many fundamental studies have been carried out to better understand the crystal structure and thermal behavior of PLLA. Multiple melting peaks have been observed in PLLA[7–13] especially in fiber form.[4,14–16] Three main mechanisms, namely, melt-recrystallization, dual (or multiple) lamellae population, and dual (or multiple) crystal structure have been suggested as the origin of multiple melting peaks of semicrystalline PLLA.[7–13] The melt-recrystallization mechanism deals with melting of the original crystals and then their recrystallization to more perfect crystals during heating scan. The dual (or multiple) lamellae population associates the formation of different morphologies before the heating scan, which may also lead to the multiple melting peaks. In the case of polymorphic polymer, the existence of two crystal forms may also lead to the appearance of double melting peaks.[11] Because the melting peaks usually overlap in the DSC curves, it is impossible, in some cases, to reveal the actual melting mechanism of the polymer structure only based on the DSC results.[7]

In combination with DSC, spectroscopy and diffraction methods provide further evidences to elucidate the structure. Both WAXD patterns and FTIR spectra have been widely applied to reveal the type of crystal structure and conformational changes of macromolecules during processing. FTIR spectroscopy is highly sensitive to the chain conformation and packing. Therefore, it is used to study the complex melting behavior and crystal structure of PLLA[7] via band assignments.[17–28] In general, three crystallization-sensitive regions can be recognized in the FTIR spectra of PLLA: The C=O stretching band of 1860–1660 cm^{-1}, the CH_3, CH bending, and C—O—C stretching band of 1500–1000 cm^{-1}, and the skeletal stretching and CH_3 rocking band region of 970–850 cm^{-1}.[17–28] The investigation of these three regions, especially the region of 970–850 cm^{-1}, resolved the helical conformation and crystal structure of PLLA.

The crystal structure of PLLA was also investigated by WAXD patterns.[4,5,29–34] However, for PLLA fibers, the powder diffraction patterns of α and β forms were quite similar, which complicated their identification.[32] The two crystal modifications can be easily distinguished only by WAXD fiber patterns, where the α form shows sharp reflections and the β form produces diffuse reflections seen as smeared layer lines in the diffraction patterns.[4]

In the last decade, the morphology, thermal, and mechanical properties along with the degradation characteristics of PLLA fibers have been intensively investigated. However, considerable numbers of the contributions have been devoted to the production and characterization of PLLA fibers and less attention has been paid to the fiber structure-property relations. In this article, as a first part of the research work, the structure, crystallinity, and thermal behavior of two PLA multifilament yarns have been characterized with three complementary techniques and rationalized with the currently presented structural models. In the second part, the physical and mechanical properties of two PLA multifilament yarns will be described.

EXPERIMENTAL

Materials

The two PLA multifilament yarns produced by a Taiwanese and a Japanese manufacturer were supplied by a research institute. The samples were abbreviated by *T* and *J*, and processed in amorphous and semicrystalline states. The crystallization was conducted at 120°C for 30 min in vacuum and the corresponding samples were designated by T_C and J_C. For making an amorphous sample, however, dried PLA filaments were sandwiched between glass plates using Teflon® spacer. Then, the sandwiched sample was held at 210°C for 10 min to ensure complete melting and then quenched in ice water.

Measurements

Thermal analyses were carried out using a TA Instrument 2010 differential scanning calorimetry (DSC) under nitrogen purge. For each heating rate, the temperature and heat flow were calibrated by indium. The samples (4–5 mg) were sealed in aluminum pans and heated from 30°C to 210°C at three rates of 5, 10, and 20°C/min. They were held at

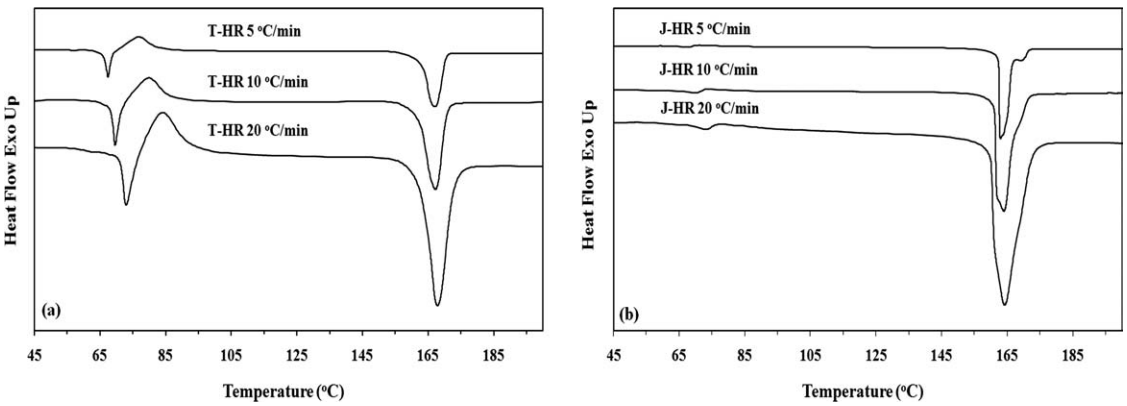

Figure 1 DSC first heating curves of the *T* (a) and *J* (b) samples at different rates.

210°C, very close to the equilibrium melting temperature of PLLA,[35,36] for 5 min under the nitrogen atmosphere to omit any crystal nuclei and forbid considerable thermal degradation. The samples were then cooled at 5, 10, and 20°C/min to 40°C and after being held for 10 min, were reheated to 200°C at heating rates of 5, 10, and 20°C/min. From DSC curves, the melting and crystallization temperatures were determined. The crystallinity ($X_{c(\mathrm{DSC})}$) was also calculated by eq. (1)[11]:

$$X_{c(\mathrm{DSC})}(\%) = 100 \times \left|\sum \Delta H_m(T_m) + \sum \Delta H_{\mathrm{cc}}(T_{\mathrm{cc}})\right| / \Delta H_m^{\circ}(T_m^{\circ}) \quad (1)$$

Where $\Delta H_m(T_m)$ and $\Delta H_{\mathrm{cc}}(T_{\mathrm{cc}})$ represent the enthalpy of fusion and crystallization at melting and crystallization temperature, respectively, and $\Delta H_{\mathrm{m}}^{\circ}(T_{\mathrm{m}}^{\circ})$ is the heat of fusion of fully crystalline sample at equilibrium melting temperature. For the heat of fusion of perfect infinite crystal, $\Delta H_{\mathrm{m}}^{\circ}(T_{\mathrm{m}}^{\circ})$, different values have been introduced in the literatures: 93.6 J g^{-1},[37] 106 J g^{-1},[38] 135 J g^{-1}.[32] In this research, the value of 93.6 J g^{-1} was used in the calculations.

Infrared spectra of the PLA samples were recorded on a Nicolet Nexuse FTIR spectrometer. Normal transmission mode was taken for the IR measurements. The spectra were obtained by coadding 40 scans at a 2 cm^{-1} resolution. Peak-fitting procedure of a commercial software package (PeakFit®) was used for the analysis of the overlapped spectral bands with a Gaussian-Lorentz function. Second derivatives of the spectra were smoothed with an 11-point Savitzky-Golay smoothing filter.

Wide angle X-ray diffraction (WAXD) patterns of the PLA filaments were recorded on a Siemens D 5000 diffractometer equipped with a CuKα (λ = 1.5405 Å) source, working at 40 kV and 30 mA. Scans were made between 5° and 40° diffraction angles at a rate of 1°/min. Diffraction peak positions was resolved by means of PeakFit® program. In this study, a Gaussian function was chosen to analyze the X-ray diffraction peak patterns. Apparent crystal size $D_{(hkl)}$ was estimated from the half breadth of the 2θ peak by using the Scherrer's Equation:

$$D_{(hkl)}(\text{Å}) = \frac{K\lambda}{\beta \cos\theta} \quad (2)$$

Where β represents full breadth at half-maximum intensity in radian, *K* is a Scherrer's constant (0.94), θ is the Bragg's angle, and λ is the wavelength of the X-ray.

RESULTS AND DISCUSSION

Thermal behavior

Figure 1 shows DSC first heating scans of the *T* and *J* samples at 5, 10, and 20°C/min. The extracted thermal properties (T_g, T_{cc}, and T_m) of the characterized samples at heating rate of 10°C/min are comparable with the literature data,[14,15] Table I. The thermal behavior of the samples also changes by the heating rate, Figure 1. Besides the glass transition temperature (T_g) and an endothermic melting peak, an enthalpy relaxation was also found for the *T* sample around T_g along with an exothermic cold crystallization peak.

The glass transition temperature of both samples was located around 68°C, which is slightly higher than the reported literature data (54–64°C) for PLLA fibers.[14–16] The observed differences can be assigned to the different molecular weight, degree of molecular orientation and crystallinity or the details of T_g measurement. The endothermic peak around T_g of the *T* sample is related to the molecular relaxation or physical aging due to its nonequilibrium characteristics.[39,40] It is noteworthy that the enthalpy recovery of the endothermic peak depends on the segmental relaxation toward the equilibrium state

TABLE I
Thermal Transitions, Enthalpies of Crystallization and Fusion Observed for the Samples (Heating Rate of 10°C/min)

Code	T_g (°C)	T_{cc} (°C)[a]	ΔH_{cc} (J/g)	T_{mc} (°C)[b]	T_m (°C)	ΔH_m (J/g)
1st scan						
T	68	80	19	–	167	43.3
J	67	–	–	–	164	48.7
2nd scan						
T	61	109	32.4	153	169	38.0
J	60	102	20.5	152	168	40.3

[a] T_{cc} indicates cold crystallization temperature.
[b] T_{mc} indicates melt-recrystallization temperature.

during heating process. Crystallinity is an important factor affecting the glass transition dynamic and enthalpy relaxation behavior through confining the segmental mobility of amorphous phase.[41] He et al.[41] and Mano et al.[39] reported an endothermic peak at 67°C with higher enthalpy recovery for nearly amorphous PLLA and lower enthalpy recovery around 70°C and 75°C for nonisothermal and isothermal crystallized samples, respectively. The increase of cooling rate enhanced the endothermic peak intensity and the T_g values of the samples at the second scans because of the crystallinity and morphological differences developed at various rates. In addition, the *T* sample displayed a crystallization exotherm immediately after T_g, whereas it was not observed for *J* sample probably due to its more isotropic amorphous structure. The morphological studies on PLLA fibers by Aou et al.[42] indicated shrinkage and cold crystallization as two events that may occur along with each other in the deformed amorphous chains through the heating process. However, nucleation-enhanced crystallization has a major effect on the post-T_g exotherm. The observed post-T_g nucleation-enhanced crystallization revealed the deformed oriented amorphous chains in the nearly amorphous *T* sample. This exothermic peak in higher crystalline *J* sample appeared with minute intensity. In fact, calorimetric studies indicated two relaxed and deformed amorphous phase in the samples.

Double endothermic melting peaks have been observed in PLLA fibers and are attributed to the initial melt spinning and subsequent drawing process.[4,14–16] Double endothermic peaks were observed for the *J* sample heated at 5°C/min, Figure 1(b). The lack of exothermic peak between the double melting peaks indicated simultaneous existence of unstable and recrystallized lamella. It seems that in competing melting and recrystallization of imperfect crystals, the rate of melting overcame the rate of recrystallization. Upon increasing the heating rate to 10°C/min and 20°C/min, the melting peak at higher temperature appeared as a shoulder and eventually merged into the low temperature peak. However, the *T* sample showed a quite different thermal behavior. It had only one endothermic peak at various applied heating rates, Figure 1(a). The melting temperatures of the *T* and *J* samples did not change considerably with applied heating rates. The observed melting temperatures for the samples were lower than reported values for β and α crystals of PLLA fibers.[4,5,43] As it was observed in the previous literature,[14,15] the DSC data of the *T* and *J* samples confirm the formation of crystals with different sizes during the processing and heating in DSC.

The enthalpy of crystallization and fusion (ΔH_{cc} and ΔH_m) of the *T* and *J* samples, extracted from Figure 1, are also presented in Table I. The developed crystalline structure of the *T* sample via the crystallizable oriented chains was transformed into the crystalline regions during the heating scan. The post-T_g cold crystallization of *T* sample indicated slight enthalpy (ΔH_{cc}) decrease and cold crystallization temperature (T_{cc}) increase with rising the heating rate Figure 1(a). The physical process of ΔH_{cc} has been characterized by nucleation-enhanced crystallization.[42] In other words, the experimental data confirm the lower crystallinity of the *T* sample and its thermal crystallization due to its deformed amorphous chains. Moreover, the *J* sample crystallized more than the *T* sample during the processing and formed small or imperfect crystals.

The nonisothermal crystallization behavior of both samples from the equilibrium molten state (210°C) was also studied by DSC at different cooling rates, Figure 2. Single exothermic peak indicates crystallization via a single process. At different applied rates, the *J* sample crystallized more than the *T* sample. In addition, crystallization temperature (T_c), heat of crystallization (ΔH_c), and crystallinity of the samples decreased with cooling rate increase. The application of higher cooling rates made the exothermic crystallization peak broaden and finally disappear. Cooling rate decrease also caused the exothermic cold crystallization peak to disappear

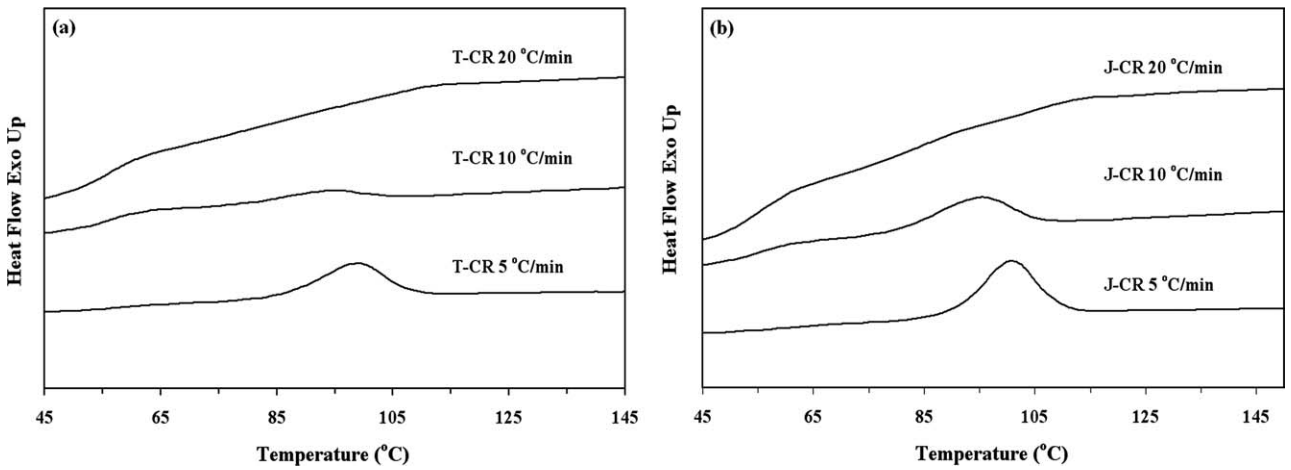

Figure 2 DSC curves of the *T* (a) and *J* (b) samples at different cooling rates.

once during the second heating scan of the samples, Figure 3.

The second heating scan may elucidate the structural reorganization of crystals leading to double melting behavior. In both samples, the appearance of double melting peaks suggests the rate of melting overwhelmed the rate of recrystallization. The disappearance of double melting peaks or appearance of exothermic peak can be attributed to simultaneous melting and recrystallization with higher recrystallization rate.[8–11] Depending on the cooling and heating rates, a weak exothermic or endothermic peak appeared before the main endothermic melting peak in DSC curves, Figure 3. Using cooling rate of 10°C/min, the exothermic cold crystallization peak appeared at about 109°C for the *T* and 102°C for the *J* sample during heating scan, Figure 3(a,b), respectively. For rapid cooling of 20°C/min, however, the temperatures corresponding to exothermic peaks were shifted to 120°C and 116°C for the *T* and *J* samples, respectively, due to the low crystalline content of the rapidly cooled samples. In other words, unstable and imperfect crystals formed during high cooling rate began to reorganize during cold recrystallization. Therefore, in DSC curves at high heating rate, a broad cold crystallization peak and single endothermic melting peak or two broad and overlapping peaks appeared.

Besides the effect of cooling and heating rates, the melting and cold crystallization behavior strongly depend on the molecular chain structure. The *T* sample with low crystalline content achieved in the cooling scan crystallized more than the *J* sample with higher melting temperature during the second heating scan. In the other words, the *J* sample crystallized further during the melt crystallization process and the *T* sample reorganized further during the second heating scan.

It is clear that the crystallization and melting mechanisms cannot be usually elucidated by the extracted data from one technique. Therefore, complementary techniques are required to cast a better

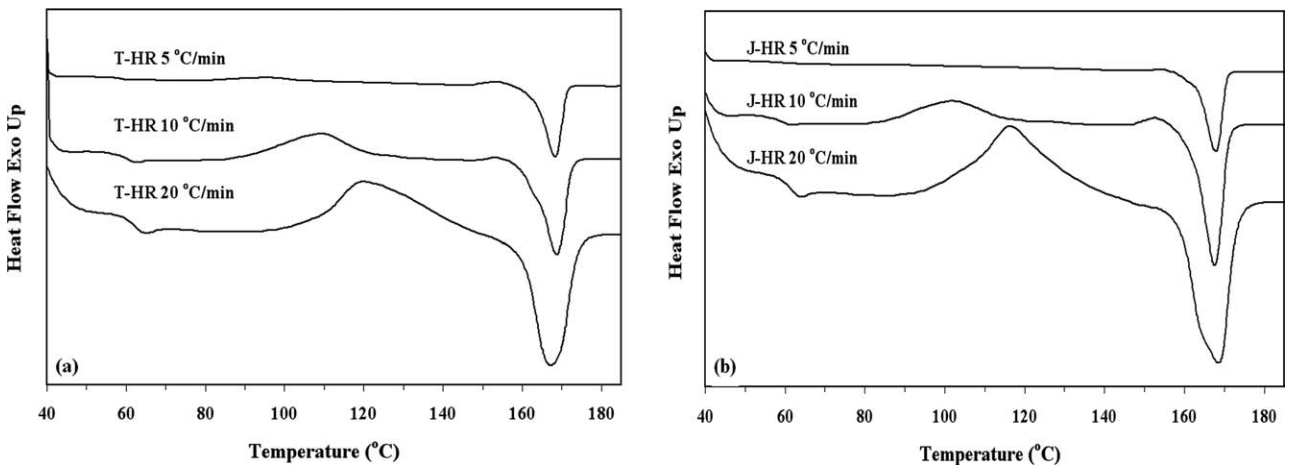

Figure 3 DSC second heating curves of the *T* (a) and *J* (b) samples at different rates.

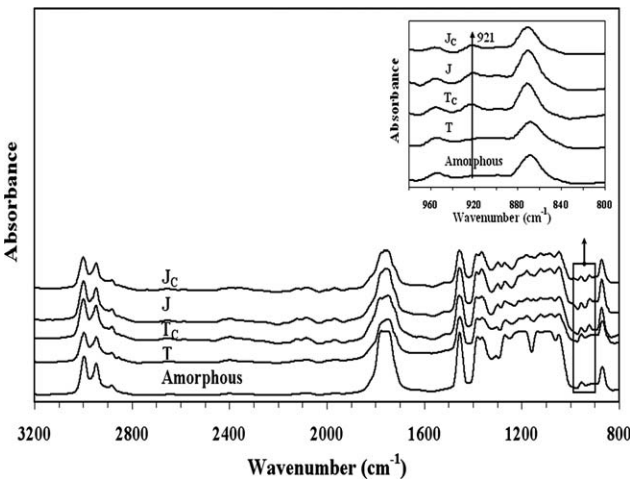

Figure 4 FTIR spectra of the amorphous, T, T_C, J, and J_C samples in the 3200–800 cm^{-1} region.

image regarding the PLA crystallization and melting.

FTIR analysis

Figure 4 displays the FTIR spectra of the amorphous, crystallized, and original samples studied in the present work in the 3200–800 cm^{-1} region. Table II compares the bands assignments collected from the literature and those bands of this research. Almost all of the observed bands in the T and J samples corresponded to the bands assigned or cited in the previous works by different investigators.[17–28] The differences between wavenumbers assignments in the literature and those bands of the samples in this study do not exceed more than 4 cm^{-1} except for the bands in C=O stretching region that are very broad and represent the molecular conformations. It should be stated that most of the wavenumbers assignments in the literature were obtained from the spectra of the PLLA films while our samples were in the filament form. Only a few very weak bands were observed in the crystalline samples in 2800–2000 cm^{-1} region that are not mentioned in the literature. These weak bands may appear due to the sample geometry or the small thickness of the filaments.

IR spectra of the PLA samples signify differences due to the crystallization. Three crystallization-sensitive regions mentioned in the introduction can be recognized for the samples prepared at different conditions. The enlarged spectral region of 1000–800 cm^{-1} is also plotted as the inset in Figure 4. The spectra were normalized using the intensity of CH_3 band around 1455 cm^{-1} and shifted vertically for easier differentiation. This band assigned to the CH_3 asymmetric deformation mode was taken as an internal standard.[17] The enlarged 1000–800 cm^{-1} region of the spectra indicates the intensity change of 921 cm^{-1} band in different samples, which is associated with the coupling of C—C backbone stretching with CH_3 rocking mode. For the amorphous sample, the complete lack of 921 cm^{-1} band is shown. This absorption band has been known as the characteristic of α crystal with the distorted 10_3 helix conformation.[17–20] In this region of the spectra

TABLE II
Wavenumbers (cm^{-1}) and Vibrational Assignments of FTIR Spectra of the Samples in the 4000–400 cm^{-1} Region

(u cm^{-1})[a]	Assignments	Refs.	T (u cm^{-1})	J (u cm^{-1})
2997 M	$\nu_{as}CH_3$	17,26	2996 S	2997 S
2947 M	$\nu_{s}CH_3$	17,26	2945 S	2946 S
2882 w	νCH	17,26	2881 M	2881 M
1760 VS	ν_{as}CH=O	17,25–28	1749 VS	1749 VS
1452 VS	$\delta_{as}CH_3$	17,26,27	1453 VS	1455 VS
1348–1384 S	$\delta_{S}CH_3$	17,26,27	1383 VS	1385 VS
1368–1360 S	δ_1(CH), CH wagging (bending)	17,26,27	1362 VS	1364 VS
1315–1300 M	δ_2(CH)	17	1301 S	1297 S
1270 S	ν(CH) + ν(COC)	17,25,27	1263 S	1265 S
1215 VS–1185 VS	ν_{as}(COC) + r_{as} (CH_3)	17,25,27	1212, 1183 VS	1215, 1184 VS
1130 S	$r_s(CH_3)$	17,25,27	1130 VS	1131 VS
1100 VS–1090 sh	ν_{as}(COC)	17,25,27	1084 VS	1089 VS
1048 S	ν(C—CH_3)	17,25,27	1045 VS	1045 VS
960 w–925 w	rCH_3 + νCC	17–21	955, 921 M	955, 921 M
875 M–860 sh	νC—COO	17,21	871 S	871 S
760 S–735 sh	δC=O	17	755 S	755 S
715 M–695 M	γC=O	17	705 M	701 M
545 w	δ_1C—CH_3 + δCCO	17	505 w	510 w

VS, very strong; S, strong; M, medium; w, weak; sh, shoulder; s, symmetric; as, asymmetric.
[a] Refer to Ref. 17.

(1000–800 cm^{-1}), the most intense band is located at 871 cm^{-1} that is assigned to νC—COO stretching and also related to the 10_3 helix conformation.[21] The lack of the characteristic band at 908 or 912 cm^{-1} assigned[22–24] to the CH_3 rocking mode of β crystal (3_1 helix), definitely reflects negligible β-crystal form in all samples.

It has been found that during the crystallization process the intensity of the crystallization-sensitive band at 921 cm^{-1} increase, whereas the intensity of the amorphous band at 955 cm^{-1} decreases.[21,25,26] Hence, it is possible to determine the quantitative relative crystallinity of the PLLA samples by using the ratio of the 921 cm^{-1} and 955 cm^{-1} band.[21,26] For the examined samples, the amorphous and the crystalline bands are well-separated in the spectra and similar changes in the T_C and J_C samples are detected. In the previous work, Meaurio et al.[25] expressed the simple way to obtain crystallinity of the PLLA samples. According to their studies, the decrease of area of the 955 cm^{-1} band is synchronized with the increase of area of the 921 cm^{-1} band. Consequently, the total crystallinity of the samples is calculated simply from the percent area loss of the band at 955 cm^{-1} via eq. (3)[25]:

$$X_{c1(\mathrm{FTIR})}\% = \frac{I_0 - I_f}{I_0} \times 100 \tag{3}$$

Where I_0 represents the area of 955 cm^{-1} band in the completely amorphous sample and I_f signifies the measured area of crystalline sample at 955 cm^{-1}. Based on the previous studies, crystallinty of PLLA samples strongly depends on the area changes of 921 cm^{-1} and 955 cm^{-1} band. Because of the synchronized area changes of both crystallized and amorphous bands, the total crystallinity of the samples can be also estimated by using eq. (4).

$$X_{c2(\mathrm{FTIR})}\% = \frac{I_{921}}{I_{955} + I_{921}} \times 100 \tag{4}$$

Where I_{921} and I_{955} indicate the area of the crystalline and amorphous bands, respectively. The total crystallinities of the T and J samples obtained through different ways are presented in Table III. For the T sample, 921 cm^{-1} band appeared as smeared line in the absorption spectrum, consequently measurement of the crystallinity became indistinguishable via eq. (4). As expected, there is reasonable agreement between results obtained from the equations.

The differences in the crystallinities of both samples from two DSC and FTIR techniques (Table III) are due to the facts that, these techniques detect different aspects of the crystalline structure that may not be determined with the other alternatives. IR spectroscopy is sensitive to the chain conformation or rotational conformers in the crystalline or disordered regions. It can measure the short-range order, which can exist without the presence of long-range order, whereas DSC is sensitive to the change in the thermal energy that depends on the meta-stable states of the fiber structure. It responds to three-dimensional order of the crystalline structure and measures the long-range order.[21,25] Because of the different values obtained for the enthalpy of fusion of the perfect crystal, different crystallinities are estimated by DSC.

TABLE III
Crystallinity of the Samples Measured by Different Techniques

Code	$X_{c(\mathrm{DSC})}$ (%)	$X_{c1(\mathrm{FTIR})}$ (%)	$X_{c2(\mathrm{FTIR})}$ (%)
T	26	20	–
J	52	42	56

The carbonyl stretching region of PLLA is very sensitive to specific interactions and/or conformational changes occurring during the crystallization process. The band area and band height of the C=O stretching along with the band splitting reflect the development in crystalline content of the PLLA samples. Because of the dipole–dipole coupling interactions, important spectral features attributed to the intermolecular or mainly interamolecular interactions between C=O groups have been reported in this region.[21,25,28] In the IR spectrum of semicrystalline PLLA, in 1880–1620 cm^{-1} region besides the weak bands, the dominant band assigned to the crystalline phase has been observed around 1760 cm^{-1}. The second derivative spectrum of crystallized PLLA has been indicated four components at about 1749, 1759, 1767, and 1776 cm^{-1}, which are attributed to the four possible conformers: tt, gt, tg, and gg, respectively. Because derivative techniques enhance the intensity of narrow bands, these four peaks can be easily distinguished in the second derivative spectra. The notations t and g refer to the trans and gauche planar ester C—O and O—C_α. The gt conformer has the lowest energy and corresponds to either a 3_1 or a 10_3 helix. The C=O groups orient only parallel to the helix axis (gg conformers) or perpendicular to it (gt, tg, and tt conformers).[25,28]

Figure 5 shows the enlarged spectral region of ν_{as}C=O asymmetric stretching mode of the samples. Because of the small relative intensity, splitting of the C=O stretching bands is difficult to observe. Hence, in the IR spectra of the T and J filaments, besides the weak bands that appeared as shoulder the broad asymmetric band appeared at about 1749 cm^{-1}. Obviously, as crystallization proceeds, important spectral changes were generated in the carbonyl region. For the T_C and J_C samples, splitting

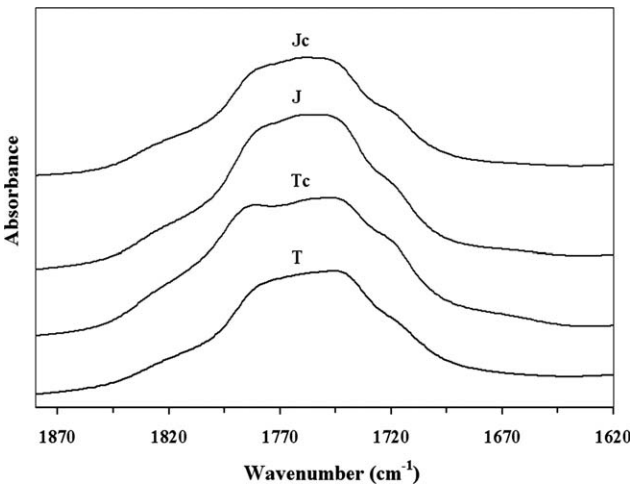

Figure 5 FTIR spectra of the *T*, T_C, *J*, and J_C samples in the 1880–1620 cm^{-1} region.

in the C=O stretching region became more evident to detect. The dominant crystalline band appeared sharp and narrow with small-wavenumber shift to 1752 cm^{-1}. It was demonstrated that the analysis of the initial spectra of PLLA samples is not suitable for the explanation the spectral changes especially in the C=O stretching region.[21] In this case, it seems necessary to utilize the other conventional spectral analysis methods such as second derivative. This technique provides information about the conformational population.[25,28]

Second derivative spectrum of the *T* sample showed four components at about 1715, 1743, 1782, and 1822 cm^{-1}. However, for the *J* sample the location of these bands shifted to 1717, 1745, 1782, and 1825 cm^{-1}, respectively. It seems that the observe bands are corresponded to the four mentioned conformers (tt, gt, tg, and gg) whit high-wavenumber shifts. The evaluation of the observed bands in the second derivative spectra indicates the different distribution of conformer in the *T* and *J* samples, which is attributed to their different crystallinity. The second derivative spectrum of amorphous PLLA sample analyzed by Meaurio et al.[25] showed two broad bands at about 1755 cm^{-1} and 1776 cm^{-1}. These bands were assigned to the two dominant conformer (gt and gg). Significant spectral differences were observed in comparing the second derivative spectrum of the *T* and cited amorphous sample in this region (1880–1620 cm^{-1}). The number and relative intensity of the splitted bands revealed the different distribution of conformer and crystallinity of the *T* sample.

The FTIR spectral of the samples in 1500–1000 cm^{-1} region, which is highly sensitive to the crystallization, are presented in Figure 6. The bands in this region were extremely overlapped; hence, the second derivative was also used to determine the band positions. The progress of crystallization has been followed by the intensity changes or frequency shifts of the bands in this region.[27] In the pervious studies, it has been noted that a band around 1454 cm^{-1} assigned to the CH_3 asymmetric deformation shows only slight wavenumber shift and intensity increase during the crystallization. Therefore, it has been taken as an internal standard.[17,27] For the amorphous and *T* sample, the CH_3 asymmetric deformation mode appeared at 1453 cm^{-1} and for the *J* sample; this band was located at 1455 cm^{-1}. For the amorphous and semicrystalline PLLA samples, the band related to the CH_3 symmetric deformation mode was detected around at 1383 cm^{-1} and 1386 cm^{-1} and the band associated with the combination of δ_1(CH) and $\delta_S CH_3$ bending appeared at 1363 cm^{-1} and 1368 cm^{-1}, respectively.[21] During the cold crystallization, small spectral changes occur for these bands. For the *T* and *J* samples, CH_3 symmetric deformation band appeared at 1383 cm^{-1} and 1385 cm^{-1}, whereas it shifts to 1386 cm^{-1} for the T_C and J_C samples. The combination δ_1(CH) and $\delta_S CH_3$ bending band appeared at 1363 cm^{-1} and 1365 cm^{-1} for the *T* and *J* samples, whereas it shifted to 1368 cm^{-1} for the T_C and J_C samples. The band assigned to the symmetric C—O—C stretching mode observed at 1212 cm^{-1} for *T* sample, shifted to 1215 cm^{-1} for the *J* sample. The band observed near 1084 cm^{-1} and 1089 cm^{-1} for the *T* and *J* samples reflect asymmetric C—O—C stretching mode. Two other bands appeared around 1130 cm^{-1} and 1045 cm^{-1} for the *T* and *J* samples are assigned to the $r_S(CH_3)$ symmetric rocking and ν(C—CH_3) stretching, respectively.[17] When comparing the results in 1500–1000 cm^{-1} region with the literature results showed

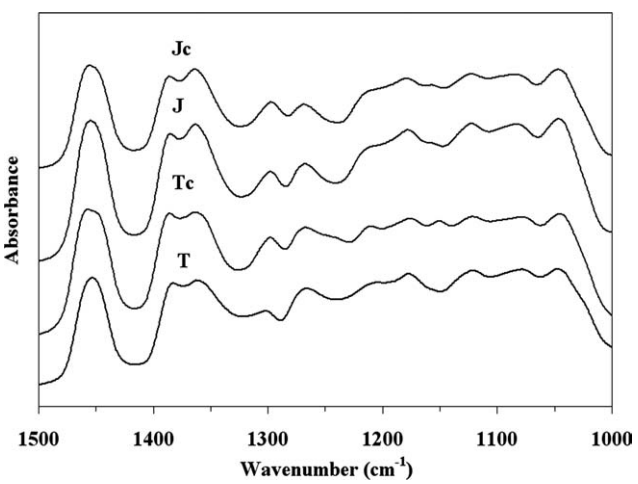

Figure 6 FTIR spectra of the *T*, T_C, *J*, and J_C samples in the 1500–1000 cm^{-1} region.

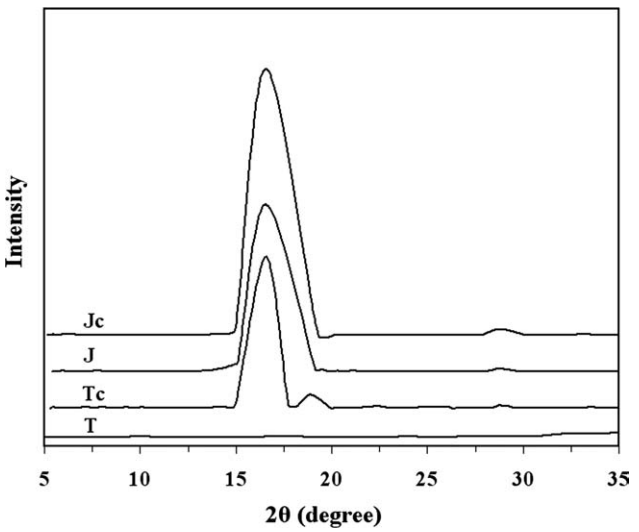

Figure 7 WAXD patterns of the *T*, T_C, *J*, and J_C samples.

that the *T* sample is not highly crystalline compared with the *J* and crystalline T_C and J_C samples.

X-ray diffraction

The structure and crystallinity of the filaments were also studied by WAXD, Figure 7. Significant differences in the WAXD patterns of the *T* and *J* samples are observed. For the *J* sample, two diffraction peaks are dominant at $2\theta = 16.5^\circ$ and 28.7°. The intense diffraction peak at lower 2θ corresponds to the Miller indices (200) and/or (110) and the weaker peak at higher 2θ is assigned to (300) planes. Because of the cold crystallization process, the intensity of these peaks increased for the J_C sample. Application of PeakFit® program led to recognition of two small diffraction peaks at 14.7° and 19.2°, which represent the (010), and (111) planes, respectively. These diffraction peaks are in agreement with the peaks reported at 15°, 16°, 18.5°, and 22.5° by Ikada et al.[29] for α crystalline structure, which consists of two 10_3 helices.[3] Apparent crystal size in the perpendicular direction to (200) planes was determined for the crystalline *J*, T_C, and J_C samples according to the eq. (2). For the *J* and J_C samples, the crystal thickness was approximately estimated to be equal to 115 Å and 154 Å, respectively. It was indicated that the crystallization improved the average crystal size in this direction.

The WAXD pattern of the *T* sample was similar to the diffraction pattern of an amorphous sample. No sharp crystalline peaks appeared and just a broad diffraction pattern with the highest intensity at $2\theta = 16.6^\circ$ was observed indicating the absence of significant crystalline order. Probably due to the low crystallinity, the crystalline reflections were weak and submerged in the amorphous scattering. Upon heating, the crystallization of the *T* sample led to the change of diffraction pattern. By means of the PeakFit®, the WAXD pattern of the T_C sample showed some diffraction peaks at $2\theta = 14.9^\circ$, 16.5°, 18.9°, 22.3°, and 28.8°. Based on the literature, the reflection at $2\theta = 14.9^\circ$ may corresponds to (010) planes, $2\theta = 16.5^\circ$ corresponds to (110) and/or (200) planes, $2\theta = 18.9^\circ$ corresponds to (111) planes, $2\theta = 22.3^\circ$ corresponds to (102) and/or (210) planes and $2\theta = 28.8^\circ$ corresponds to (300) planes.[29,34] These results confirm the α crystal growth in the isothermal crystallization of the *T* sample. For the T_C sample, the crystal size in perpendicular direction to the (200) planes was approximated to be equal to 184 Å.

CONCLUSIONS

The performance of PLLA fiber in textile industry can be extended by understanding its structure-property relations. The thermal and mechanical properties of the fibers greatly depend on the structure and morphology. In this study, two PLA multifilament yarns from two different manufacturers were characterized with regard to the thermal properties and structure based on the DSC, FTIR, and WAXD. The FTIR results, DSC, and WAXD data strongly indicated only α form crystal structure for the crystalline filaments. However, two PLA multifilament yarns exhibited significant differences in their crystalline content, thermal properties, and amorphous phase structure.

The detailed analysis of crystallization-sensitive FTIR regions provided information about chain conformers and crystallinty of the filaments. The crystallinity of the filaments were determined from intensity of the crystalline band, which are related to the 10_3 helix conformation and skeletal amorphous band in the 970–850 cm^{-1} region. The crystalline content of the filaments, which were calculated from DSC curves were comparable with those from FTIR and qualitatively confirmed the WAXD results.

The recrystallization and melting of the recrystallized and original crystals, led to the appearance of double melting peaks during the heating of semicrystalline filament in DSC. Because of the higher crystalline content, it did not show cold crystal growth in comparison with low crystalline filament. Nearly amorphous filament indicated enthalpy relaxation around T_g and post-T_g nucleation-enhanced crystallization during heating in the DSC, which confirmed the existence of highly deformed chains in the amorphous phase.

The authors thank Prof. S. C. Yao and Prof. J. H. Lin from Taiwan Textile Research Institute for supplying the PLA multifilament yarns used in this research. They also thank

Dr. Karimi at the Thermal Analysis laboratory at Amirkabir University allowing us to use of DSC and FTIR instruments.

References

1. Garlotta, D. J. J Polym Environ 2002, 9, 63.
2. Gupta, B.; Revagade, N.; Hilborn, J. Prog Polym Sci 2007, 32, 455.
3. De Santis, P.; Kovacs, A. J. Biopolymers 1968, 6, 299.
4. Eling, B.; Gogolewsky, S.; Pennings, A. J. Polymer 1982, 23, 1587.
5. Hoogsteen, W.; Postema, A. R.; Pennings, A. J.; ten Brinke, G.; Zugenmaier, P. Macromolecules 1990, 23, 634.
6. Cartier, L.; Okihara, T.; Ikada, Y.; Tsuji, H.; Puiggali, J.; Lotz, B. Polymer 2000, 43, 8909.
7. Pan, P.; Kai, W.; Zhu, B.; Dong, T.; Inoue, Y. Macromolecules 2007, 40, 6898.
8. Yasuniwa, M.; Tsubakihara, S. H.; Sugimoto, Y.; Nakafuku, C. J Polym Sci Part B: Polym Phys 2004, 42, 25.
9. Di Lorenzo, M. L. J Appl Polym Sci 2006, 100, 3145.
10. Di Lorenzo, M. L. Macromol Symp 2006, 234, 176.
11. Ling, X.; Spruiell, J. E. J Polym Sci Part B: Polym Phys 2006, 44, 3200.
12. Yasuniwa, M.; Iura, K.; Dan, Y. Polymer 2007, 48, 5398.
13. Yasuniwa, M.; Sakamo, K.; Ono, Y.; Kawahara, W. Polymer 2008, 49, 943.
14. Fambri, L.; Pegoretti, A.; Fenner, R.; Incardona, S. D.; Migliaresi, C. Polymer 1997, 38, 79.
15. Mezghani, K.; Spruiell, J. E. J Polym Sci Part B: Polym Phys 1998, 36, 1005.
16. Yuan, X.; Mak, A. F. T.; Kwok, K. W.; Yung, B. K. O.; Yao, K. J Appl Polym Sci 2001, 81, 251.
17. Kister, G.; Cassanas, G.; Vert, M. Polymer 1998, 39, 267.
18. Cohn, D.; Younes, H. J. Biomed Mater Res 1988, 22, 993.
19. Lee, J. K.; Lee, K. H.; Jin, B. S. Eur Polym J 2001, 37, 907.
20. Sawai, D.; Takahashi, K.; Sasashige, A.; Kanamoto, T. Macromolecules 2003, 36, 3601.
21. Zhang, J.; Tsuji, H.; Noda, I.; Ozaki, Y. J Phys Chem 2004, 108, 11514.
22. Urayama, H.; Moon, S.; Kimura, Y. Macromol Mater Eng 2003, 288, 137.
23. Fawcett, A. H. Polym Commun 1982, 23, 1865.
24. Kang, S.; Hsu, S. L.; Stidham, H. D. Macromolecules 2001, 34, 4542.
25. Meaurio, E.; Lo'pez-Rodri'guez, N.; Sarasua, J. R. Macromolecules 2006, 39, 9291.
26. Zhang, J.; Duan Sato, Y. H.; Tsuji, H.; Noda, I.; Yan, S.h; Ozaki, Y. Macromolecules 2005, 38, 8012.
27. Zhang, J.; Tsuji, H.; Noda, I.; Ozaki, Y. Macromolecules 2004, 37, 6433.
28. Meaurio, E.; Lo'pez-Rodri'guez, N.; Sarasua, J. R. J Phys Chem B 2006, 110, 5790.
29. Ikada, Y.; Jamshidi, K.; Tsuji, H.; Hyon, S. H. Macromolecules 1987, 20, 906.
30. Okihara, T.; Tsuji, M.; Kawaguchi, A.; Katayama, K. I.; Tsuji, H.; Hyon, S. H.; Ikada, Y. J. Macromol Sci Phys 1991, 30, 119.
31. Kobayashi, J.; Asahi, T.; Ichiki, M.; Okikawa, A.; Suzuki, H.; Watanabe, T.; Fukada, E.; Shikinami, Y. J Appl Phys 1995, 77, 2957.
32. Miyata, T.; Masuko, T. Polymer 1998, 39, 5515.
33. Di Lorenzo, M. L. Eur Polym J 2005, 43, 569.
34. Yasuniwa, M.; Tsubakihara, S.; Iura, K.; Ono, Y.; Dan, Y.; Takahashi, K. Polymer 2006, 47, 7554.
35. Kalb, B.; Pennings, A. J. Polymer 1980, 21, 607.
36. Vasanthakumari, R.; Pennings, A. J. Polymer 1997, 38, 4003.
37. Fischer, W.; Sterze, H. J.; Wenger, G. Kolloid Z Z Polym 1973, 251, 980.
38. Sarasua, J. R.; Prud'homme, R. E.; Wisniewski, M.; Le Borgne, A.; Spassky, N. Macromolecules 1998, 31, 3895.
39. Mano, J. F.; Go'mez Ribelles, J. L.; Alves, N. M.; Salmero'n Sanchez, M. Polymer 2005, 46, 8258.
40. Pan, P.; Zhu, B.; Inoue, Y. L. Macromolecules 2007, 40, 9664.
41. He, Y.; Fan, Z.; Hu, Y.; Wu, T.; Wei, J.; Li, S. Eur Polym J 2007, 43, 4431.
42. Aou, K.; Kang, S.; Hsu, S. L. Macromolecules 2005, 38, 7730.
43. Motes De Oca, H.; Ward, I. M. J Polym Sci Part B: Polym Phys 2007, 45, 892.